A critical evaluation of decadal solar cycle imprints in the MiKlip historical ensemble simulations

Tobias C. Spiegl[1], Ulrike Langematz[1], Holger Pohlmann[2], Jürgen Kröger[2]

[1]Institute of Meteorology, Freie Universität Berlin, Berlin, Germany

[2]Max Planck Institute for Meteorology, Hamburg, Germany

Correspondence to: T. C. Spiegl (tobias.spiegl@met.fu-berlin.de)

hat gelöscht: A

Abstract

Studies concerning solar-terrestrial connections over the last decades claim to have found evidence that the quasi-decadal solar cycle can have an influence on the dynamics in the middle atmosphere in the Northern Hemisphere during winter season. It has been argued that feedbacks between the intensity of the UV part of the solar spectrum and low latitude stratospheric ozone may produce anomalies in meridional temperature gradients which have the potential to alter the zonal-mean flow in mid to high latitudes. Interactions between the zonal wind and planetary waves can lead to a downward propagation of the anomalies, produced in the middle atmosphere, down to the troposphere. More recently, it has been proposed that top-down initiated decadal solar signals might modulate surface climate and synchronize the North Atlantic Oscillation. A realistic representation of the solar cycle in climate models was suggested to significantly enhance decadal prediction skill. These conclusions have been debated controversial since then due to the lack of missing realistic decadal prediction model set ups and more extensive analysis.

In this paper we aim for an objective and improved evaluation of possible solar imprints from the middle atmosphere to the surface and with that from head to toe. Thus, we analyze model output from historical ensemble simulations conducted with the state-of-the-art Earth system model MPI-ESM-HR. The target of these simulations was to isolate the most crucial model physics to foster basic research on decadal climate prediction and to develop an operational ensemble decadal prediction system within the MiKlip framework.

Based on correlations and multiple linear regression analysis we show that the MPI-ESM-HR simulates a realistic, statistically significant and robust shortwave heating rate and temperature response at the tropical stratopause, in good agreement with existing studies. However, the dynamical response to this initial radiative signal in the NH during the boreal winter season is weak. We find a slight strengthening of the polar vortex in midwinter during solar maximum conditions in the ensemble mean, which is consistent with the so-called "top-down" mechanism. The individual ensemble members, however, show a large spread in the dynamical response with opposite signs in response to the solar cycle, which might be a result of the large overall internal variability compensating rather small solar imprints.

We also analyze the possible surface responses to the 11-year solar cycle and review the proposed synchronization between the solar forcing and the North Atlantic Oscillation. We find that the simulated westerly wind anomalies in the lower troposphere as well as the anomalies in the mean sea level pressure are most likely independent from the timing of the solar signal in the middle atmosphere and the alleged top-down influences. The pattern rather reflects

55 the decadal internal variability of the troposphere, mimicking positive and negative phases of the Arctic- and North

56 Atlantic Oscillations throughout the year sporadically, which is then assigned to the solar predictor time series without

57 any physical plausible connection and sound solar contribution.

58 Finally, by applying lead/lag correlations, we find that the proposed synchronization between the solar cycle and the

59 decadal component of the North Atlantic Oscillation might rather be a statistical artefact, affected for example by the

60 internal decadal variability of the ocean, than a plausible physical connection between the UV solar forcing and quasi-

61 decadal variations in the troposphere.

62

71 1. **Introduction**

72 The discipline of decadal climate prediction is rather young and a rapidly growing field in climate science. By using

73 initialized climate model simulations, the gap between weather forecasting and long-term climate model projections

74 covering the complete 21st century or beyond is bridged (e.g., Pohlmann et al., 2013; Meehl et al., 2014). By the aid

75 of decadal climate predictions, policymakers can be equipped with an improved decision-making basis allowing for a

76 better planning of necessary water resources, agriculture, energy and infrastructure measures for the near-term future

77 (Mehta et al., 2011). The aim of the German joint research project "Mittelfristige Klimaprognose" (MiKlip) was to

78 establish a new decadal prediction system allowing for a more precise midterm climate forecasting. To this effect,

79 potential driving factors shaping the decadal climate from both anthropogenic and natural sources have been evaluated

80 critically based on large ensemble simulations with the Max Planck Institute for Meteorology Earth System Model

81 (MPI-ESM).

82 One factor that potentially influences tropospheric weather and climate is the variability in the middle atmosphere via

83 stratosphere-troposphere coupling processes. The internal variability in the middle atmosphere during the dynamically

84 active winter and spring seasons is strongly controlled by the variability of Rossby waves, which propagate upward

85 from the troposphere to the middle atmosphere where they break and interact with the zonal-mean flow. The changes

86 in the zonal-mean flow, again, can alter the propagation conditions for planetary scale waves initiating a self-consistent

87 feedback called wave-mean flow interaction (e.g. Andrews 1985). As a result, strong disruptions, born in the middle

88 atmosphere, such as sudden stratospheric warmings (SSWs), which are characterized by a breakdown of the polar

89 vortex, have the potential to propagate downward into lower atmospheric layers and interfere with the tropospheric

90 weather regime (e.g,. Baldwin and Dunkerton, 2001). A prominent example for this are Northern Hemisphere (NH)

91 cold air outbreaks which have the tendency to be more frequent and severe in seasons with a weak stratospheric polar

92 vortex (e.g. Huang et al., 2021).

93 A source of variability that might influence the dynamics in the middle atmosphere on the decadal timescale via a

94 complex feedback mechanism between radiation, chemistry and wave-mean flow interaction is the 11-year solar cycle.

95 Pioneering work concerning the impact of the solar cycle on middle atmosphere dynamics and possible connections

96 to the troposphere goes back to Kodera and Kuroda (2002). Based on a relatively short period of NCEP reanalysis data

97 (1979 – 1998), the authors observed an increase of the tropical stratopause temperature (TST) (at ~50 km) during the

98   time of the solar maximum. In their conceptual explanation, this temperature increase leads to a strengthening of the

99   meridional temperature gradient and an intensification of the polar night jet (PNJ) in the winter stratosphere. The

100   stronger westerlies create a barrier for upward propagating planetary waves, which in turn are deflected poleward and

101   break at lower altitudes. The resulting divergence in the Eliassen-Palm flux (EPF) allows the positive wind anomaly

102   to move downward and poleward over the winter season. Kodera (2002) argues that the solar induced wind anomalies

103   may advance into the troposphere, where they create a signal in meteorological variables mimicking a positive phase

104   of the North Atlantic Oscillation (NAO). Matthes et al. (2004, 2006) studied the proposed "top-down" mechanism by

105   the aid of idealized simulations with an early 3-dimensional middle atmosphere general circulation model (GCM).

106   Analysing monthly to sub-monthly means, they found that during solar maximum conditions the polar vortex seems

107   to be stronger especially in November and December and linked this to a positive Arctic oscillation (AO)-like pattern

108   which they found in lower altitudes and to some extent at the surface. The observed pattern weakens in January and

109   changes sign from February onwards. In subsequent studies comparable results have been found (e.g., Schmidt et al.,

110   2010; Ineson et al., 2011; Chiodo et al., 2012; Langematz et al., 2013). However, the exact timing of the progression

111   of the signals from the middle atmosphere to the surface depends on the individual study and varies from December

112   to February. These early studies are often quoted as convincing proof for a "top-down" influence of the 11-year solar

113   cycle in both the middle atmosphere and the troposphere. Complementary to this, Gray et al. (2013) found that the

114   strongest NAO-like solar-induced signals in the North Atlantic (i.e. a positive phase of the NAO) actually seem to

115   appear with a time lag of three to four years after the solar maximum in the respective seasonal winter mean (DJF).

116   However, the observed lags could not be reproduced in coupled atmosphere-ocean simulations conducted by the same

117   group. In the model, the postulated response to the solar cycle in the North Atlantic appears almost in phase with the

118   solar forcing (maximum response between lag year zero to one) (Gray et al., 2013). This discrepancy between observed

119   and simulated lag in the response in the North Atlantic NAO was confirmed in subsequent studies (e.g., Scaife et al.,

120   2013; Andrews et al., 2015).

121   With respect to possible solar induced impacts on NH surface variability in the winter season, Thiéblemont et al.

122   (2015) went one step further. Analyzing a simulation incorporating 150 model years, they claim that the solar forcing

123   synchronizes the decadal component of the NAO variability spectrum, a phase relation they cannot find in an

124   experiment without 11-year solar variability. This result has been debated controversially since its publication. Chiodo

125   et al. (2019) found almost identical spectra of the NAO decadal variability in two simulations of 500 model years each,

141 with and without a 11-year solar cycle forcing. Furthermore, they identified NAO patterns in similar time segments in

142 both experiments (forced and unforced). They suspect, therefore, that the alleged surface solar signals in other studies

143 are most likely a result of the internal variability of the NAO itself rather than solar cycle imprints. On the other hand,

144 Drews et al. (2022) most recently argue that the solar cycle near-surface imprints can only shine through during very

145 active solar periods with large amplitudes of the 11-year solar cycle. They also state that during these periods the

146 surface decadal prediction skill would be significantly enhanced if the solar cycle is a vital part of the prediction

147 system. In the context of the most recent literature, it is difficult to understand why Chiodo et al. (2019) and Drews et

148 al. (2022) arrive at a different assessment of the solar signal, even though the same model was used. This might point

149 to the fact, that the complexity of the model is not the most relevant component in shaping potential surface solar

150 signals, but rather the effects of internal variability in individual model runs and (to some degree) the applied analysis.

151 In this publication, we evaluate possible imprints of the 11-year solar cycle in different domains of the atmosphere

152 from the initial solar radiative signal in the tropical upper stratosphere down to the surface in the NH winter season.

153 We analyze the MiKlip historical ensemble simulations conducted with the state-of-the-art Earth system model MPI-

154 ESM-HR, which is the physical basis for the decadal prediction system, which is operational at the "Deutscher

155 Wetterdienst" (DWD) since 2020. The availability of the large amount of output data from the MiKlip historical model

156 ensemble enables us to address the unresolved questions of the solar surface imprint, such as the dependence of the

157 signal on the solar cycle amplitude, on a more robust statistical basis than is possible in single model simulations. In

158 our study, we aim to identify the role of the solar imprints for the decadal variability of the NAO in winter. While the

159 model simulations include both, changes in the total solar irradiance (TSI) and spectral solar irradiance (SSI), potential

160 effects related to solar energetic particles (SEP) and medium energy electrons (MEE) are not explicitly included in the

161 MiKlip experiments. Observations and model studies suggest that changes in the stratospheric composition related to

162 SEP can lead to a radiatively driven modulation of the middle atmosphere dynamics, which can penetrate to lower

163 atmospheric layers down to the troposphere (e.g., Seppälä et al., 2009, 2014; Baumgaertner et al., 2010; Arsenovic et

164 al., 2016). However, since no robust surface impacts have been simulated even for strong solar energetic particle

165 events (SEP) of the recent decades (Jackman et al., 2009), we infer that including these effects may not alter our results

166 significantly.

167 This publication is structured as follows. In Section 2 we describe the MPI-ESM, the setup of the analyzed simulations

168 and the applied methodologies to detect potential solar cycle signals in different atmospheric domains. In Section 3,

169 the initial radiative solar signal in the tropical middle atmosphere is evaluated. Subsequently, we concentrate on the

170 dynamical response to the initial solar signal in the NH winter season. Here we show in Section 4 the ensemble mean

171 response and compare individual ensemble members with opposite solar signatures. In Section 5, we derive solar-

172 induced signals near the surface in our simulations and observations. In Section 6, we check our model results with

173 respect to the proposed synchronization between the solar forcing and the NAO. Finally, we summarize and discuss

174 our results in a broader context (Section 7).

175

2. **Data and methods**

177 2.1 Model description and experimental design

178 The historical simulations analyzed in this publication have been conducted with the Max Planck Institute for

179 Meteorology Earth System Model in high resolution configuration (MPI-ESM1.2-HR; hereafter called MPI-ESM-

180 HR) at the Deutsches Klimarechenzentrum (DKRZ). MPI-ESM-HR includes the atmospheric general circulation

181 model ECHAM (European Centre Hamburg) version 6.3 (ECHAM6.3) with a horizontal/vertical resolution of

182 T127L95 (corresponds to a ~100 km * 100 km model grid and 95 levels in the vertical with a model top at 0.01 hPa

183 or ~80 km) (Müller et al., 2018). The high vertical resolution allows for an internally generated quasi-biennial

184 oscillation (QBO) in the tropical stratosphere (Pohlmann et al., 2019). Radiative processes are represented using the

185 rapid radiation transfer model for GCMs (RRTM-G) for both the shortwave and longwave part of the electromagnetic

186 spectrum (Iacono et al., 2008). Other diabatic processes, such as vertical mixing by turbulence and moist convection,

187 large-scale convection, and momentum deposition by orographic and unresolved gravity waves are described in more

188 detail in Stevens et al. (2013). Oceanic processes are accounted for in the coupled Max Planck Institute ocean model

189 (MPIOM) with a TP0.4 (0.4° nominal) resolution (Jungclaus et al., 2013). MPI-ESM-HR further incorporates the

190 biogeochemistry module Hamburg Model of the Ocean Carbon Cycle (HAMOCC) (Ilyina et al., 2013; Paulsen et al.,

191 2017) and the land surface model JSBACH (Reick et al., 2013).

192 In this publication, we analyze 10 members of the MPI-ESM-HR historical simulations performed within the German

193 research project MiKlip. The MiKlip historical ensemble simulations include the observed natural and anthropogenic

194 climate drivers, as described in the CMIP5 protocol (Taylor et al., 2013). The individual ensemble members (1 to 10)

195 have been initialized from different model years of a 1850 preindustrial (PI) control simulation and were integrated

196   over the period 1850 to 2005. Since especially the very early years are little reliable in observations and the model has

197   been spun-up with a constant solar forcing, we focus on the period 1880 – 1999. Thus, a total of 1,200 model years

198   have been evaluated. Since the model does not include interactive atmospheric chemistry, ozone concentrations have

199   to be prescribed. In the MiKlip historical simulations, the merged CMIP5 ozone dataset was used, which consists of a

200   combination of SAGE I+II satellite and radiosonde data in the period 1979 to 2005. To derive earlier ozone

201   concentrations back to 1850, the zonal mean stratospheric time series is extended backwards based on the regression

203 fits and proxy time series of equivalent effective stratospheric chlorine (EESC) and solar variability (Cionni et al.,

204 2011). The solar variability forcing includes all observed solar cycles and follows Lean (2000).

205

206 2.1 Data analysis

207 *Detrending, correlations, filtering*

208 To detrend the sunspot number (SSN) (Source: WDC-SILSO, Royal Observatory of Belgium, Brussels -

209 https://www.sidc.be/silso/infosnmtot) and shortwave heating rate time series, a third-degree polynomial function has

210 been fitted to the data, the respective anomalies are shown in Figure 1 (the original, unfiltered SSN time series is

211 shown in Supplementary Figure 1). The detrended SSN time series has then been correlated (Pearson r) with the

212 detrended tropical stratopause temperature (defined as the mean value between 25°S – 25°N at 1 hPa (Figure 3). All

213 correlation analyses have been performed by using the Python scipy.pearsonr function. Statistical significance of the

214 correlations has been calculated by using a two-tailed Student's t-test, as implemented in Python. In this manuscript

215 we use the term "robust" if a signal of the same sign (e.g., the temperature response at the tropical stratopause)

216 appears in the majority of our ensemble members. To reduce the degree of internal variability, a Butterworth

217 bandpass filter with cutoff frequencies of 9 and 13 years has been applied to the detrended PNJ time series (defined

218 as the arithmetic mean of the zonal-mean zonal wind between 35°N – 45°N at 1 hPa) (Figure 3). The same

219 Butterworth bandpass filter has also been applied to the zonal-mean zonal wind time series at 10 hPa (zonal mean

220 over 55°N – 65°N) (Figure 3) and the NAO time series. The NAO time series has been calculated by the aid of an

221 EOF analysis conducted for the MSLP data over the Atlantic sector (20 – 80°N, 90°W – 40°E) in the winter season

222 (DJF averaged and individually for December, January and February). The first principal component is then used to

223 describe the NAO variability. The lead/lag correlations (Figure 8) are then calculated between the filtered NAO and

224 SSN time series.

225 *Multiple linear regression*

hat gelöscht: .

hat gelöscht:)

228   To detect the solar cycle signals in the middle atmosphere (Figures 2, 4 and 5) and in the mean sea level pressure in

229   both observations and model data (Figures 6 and 7), we use an established multiple linear regression (MLR) technique

230   as described in Bodeker et al. (1998). To derive the individual regression coefficients, we use a set of six predictors in

231   the MLR model:

232   $X(t) = \text{Off.const} + A * CO2(t) + B * QBO(t) + C * QBOorth(t) + D * SSN(t) + E * Nino3.4(t) + F * tau(t) + R(t)$

233   with: Off.const = annual cycle; CO2(t) = increase in the atmospheric CO_2 concentration; QBO(t) = phase of the QBO,

234   defined by the zonal-mean zonal wind in 30 hPa (5°S – 5°N); QBOorth(t) = the orthogonal of QBO(t); SSN(t) = SSN

235   time series; Nino3.4(t) = Nino3.4 times series; tau(t) = optical thickness at 550 nm and R(t) = model residuum. Based

236   on this MLR analysis, we derived the model response to our chosen set of predictors, e.g., the temperature response

237   per unit of the predictor (i.e., K per 1 SSN). To display the model response during solar maximum, we scaled the

238   coefficients to 180 SSN, which is a good approximation for a mean solar cycle amplitude between 1880 and 1999. To

239   detect potential time lags in the response to the solar cycle at the surface, the solar time series has been shifted in such

240   a way that the model response lags the solar forcing by 1 to 4 years. We like to note, that we use the raw (unfiltered)

241   model output as input for our MLR analysis.

242

243   **3.   The initial radiative solar signal in MPI-ESM**

244   The dynamical "top-down" mechanism, assumed to be the pathway for the propagation of the solar signature through

245   the atmosphere to the surface in NH winter (see also Section 1), is initiated at the tropical upper stratosphere by the

246   absorption of solar ultraviolet (UV) irradiance by ozone and molecular oxygen. In particular, the absorption of solar

247   photons by ozone in the Hartley bands (200 – 310 nm) in the upper stratosphere - and to a lesser extent the Huggins-

248   bands (310 nm – 400 nm) in the middle stratosphere – heats the upper stratosphere increasingly with height and leads

249   to the formation of the warm stratopause. Although the variation in solar UV-irradiance over the 11-year solar cycle

250   is less than 10% in the ozone absorption bands, the enhanced UV radiation at solar maximum – in combination with

251   increased ozone concentrations - leads to stronger shortwave heating and a concurrent warming of the tropical

252   stratopause by the order of 1 K, as has been derived from merged MSU4 and SSU+MLS-satellite observations (Randel

253   et al., 2016).

hat gelöscht: The solar related coefficients have been

hat gelöscht: scaled to 1

256   Figure 1a shows the annual mean response of the modelled shortwave radiative heating rate (SWHR) at the

257   stratosphere and lower mesosphere (100 – 0.1 hPa) for a range of solar cycle (SC) amplitudes from the weak SC14 (in

258   blue), over the medium SC22 which has been used as solar forcing in the CMIP5 protocol (in green), to the very strong

259   SC19 (in red). MPI-EMS-HR produces the well-known solar cycle impact with enhanced SW heating during solar

260   maximum throughout the upper stratosphere and lower mesosphere. The maximum SWHR difference develops at the

261   stratopause and ranges for the three selected solar cycles between 0.17 and 0.51 K/day. With a SWHR increase of 0.32

262   K/day for the SC22 solar forcing, MPI-ESM-HR produces an initial solar radiative response at the tropical stratopause

263   which is in very good agreement with offline radiation model calculations using the CMIP5 solar forcing (i.e., the

264   same forcing as in MPI-ESM-HR) in a line-by-line reference and two CCM (EMAC and WACCM) radiation codes

265   (see Figure 8, yellow curves in Matthes et al., 2017). This is a significant improvement compared to the earlier

266   ECHAM4 and ECHAM5 model versions which were not able to simulate the SWHR response to the solar cycle in the

267   stratosphere (see Figure 17 in Forster et al., 2011), and thus missed the initial solar temperature signal necessary for

268   the "top-down" mechanism. The improvement in the MPI-ESM-HR is the result of the enhanced spectral resolution

269   of the new shortwave radiation scheme in ECHAM6 which resolves the shortwave spectrum in 14 bands spanning the

270   wavelength range from 820 to 50,000 cm^{-1} (Iacono et al., 2008), whereas ECHAM4 and ECHAM5 used a lower

271   spectral resolution with the four-band model of Fouquart and Bonnel (1980), later extended to six bands by Cagnazzo

272   et al. (2007).

273   Figure 1b shows the time series of the SSN and the modeled SWHR at the tropical stratopause over the period from

274   1880 – 1999. The shown anomalies of both time series from a third-degree polynomial fit clearly demonstrate that

275   solar cycles of different amplitudes initiate SWHR responses that closely follow in magnitude the strength of the solar

276   forcing. Only during SC20, the maximum SWHR response is higher than expected for that weak solar cycle. This is

277   not reproduced in the SWHR, possibly due to the transition from synthetic SSN before 1979 to observed SSN

283 afterwards.
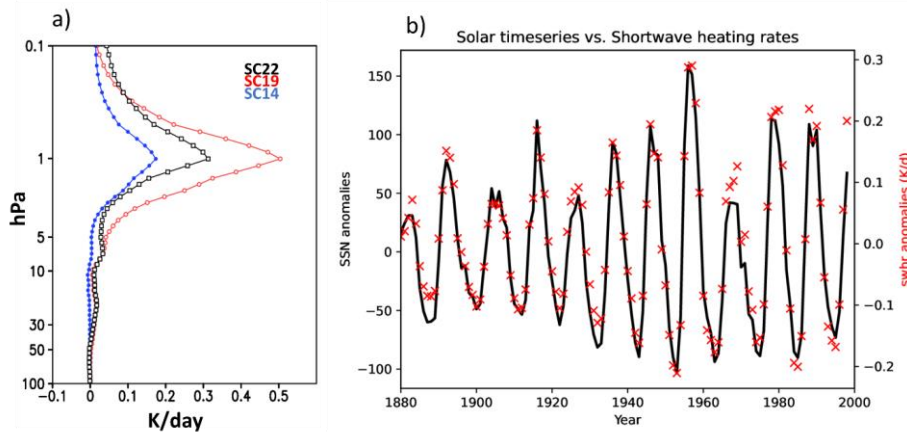
284

285 **F****igure 1:** Solar shortwave heating rate signature in the MPI-ESM-HR historical simulations: a) Annual tropical
286 mean (25°S – 25°N) shortwave heating rate difference in K/day between the maximum and minimum of three solar
287 cycles: the weak solar cycle 14 (blue), the medium solar cycle 22 used in CMIP5 (green), and the strong solar cycle
288 19 (red) (a), and: Time series of the sunspot number and the annual tropical mean (25°S – 25°N) shortwave heating
289 rate at the stratopause (1 hPa). Shown are anomalies from a third-degree polynomial fit to the data (b).
290

291 When averaging over all solar cycles between 1880 and 1999 and all 10 ensemble members, we obtain a robust, highly

292 significant annual mean warming of the complete middle atmosphere at solar maximum (Figure 2a), reaching a peak

293 response of 1.2 K at the tropical stratopause (Figure 2b). This result is slightly higher than the solar signal derived

294 from satellite observations (0.7 K / 100 solar flux units, respectively ~1 K between solar minimum and maximum)

295 (Randel et al., 2016). In our simulations we can't find the sometimes observed secondary peak in the temperature in

296 the lower stratosphere. This secondary peak, however, can no longer be found even in most recent analysis of satellite

297 data. Dhomse et al. (2022) suggest that the secondary peak (found in earlier studies) emerged most likely due to

298 aliasing effects related to the Mount Pinatubo eruption in 1991 and probably was not a result of solar variability.

299 Given the excellent temporal evolution of the initial radiative response of the upper tropical stratosphere to the decadal

300 solar forcing, we conclude that MPI-ESM-HR produces the necessary prerequisite for the dynamically enhanced "top-

301 down"-mechanism, which will be investigated in more detail in the next section.

302
303
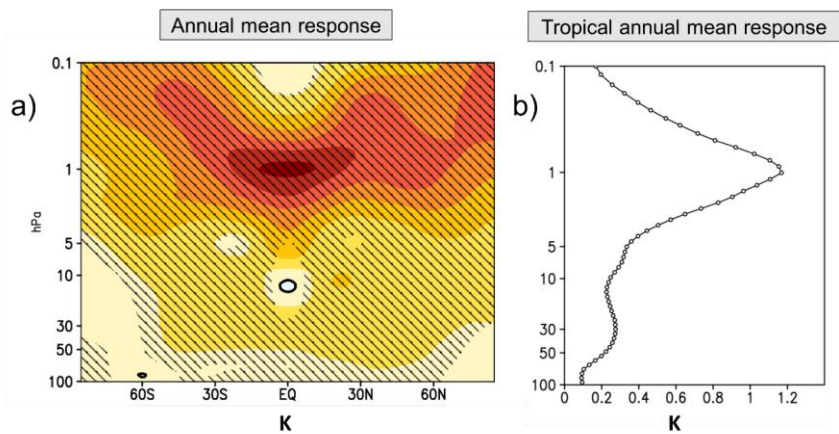
Figure 2: Long-term annual ensemble mean response based on MLR analysis of the zonal-mean temperature (in K) to the solar cycle in the middle atmosphere as a function of height and latitude (hatched regions mark 95% statistical significance) (a), and the annual mean tropical (25°S – 25°N) temperature response (in K).

4. Downward transfer of the solar signal to the surface: the key role of dynamics

After having demonstrated the ability of the MPI-ESM-HR model to realistically simulate the radiative and the related temperature response in the tropical upper stratosphere to the decadal solar forcing, we investigate as next step the potential dynamical reaction to the radiative forcing, which is expected according to the "top-down" mechanism. By evaluating the ensemble spread in the NH during the dynamically active season (November to March), we assess the variability of different dynamical variables in the stratosphere with respect to the solar fluctuations in the MPI-ESM-HR historical ensemble simulations. We focus first on the detrended deviations from the long-term monthly means for the TST and (to estimate the dynamical response in the NH) the zonal-mean zonal wind at two different altitudes and latitudes (Figure 3). To approximate the PNJ (the local maximum wind speed in the upper stratosphere) we use the mean of the zonal-mean zonal wind in 35°– 45°N at 1 hPa. The variability in the middle stratosphere is represented by the mean of the zonal-mean zonal wind in 55°– 65°N at 10 hPa. After calculating the respective anomaly time series for the TST, the PNJ and the 10 hPa zonal wind variations for each month individually, we correlate these time series with the detrended DJF mean SSN time series. To mute the interannual variability (operating on timescales between 1 and 8 years) of the polar vortex, the PNJ and 10 hPa anomaly time series, as well as the SSN time series, have been bandpass-filtered, before calculating the correlations. Please note, that the same SSN time series has been used for the correlation for all individual ensemble members, leading to a "vertical arrangement" of the data in the

339 scatter plots shown in Figure 3. Our results indicate that the TST correlates significantly with the SSN, not only in the

340 annual mean (compare Figure 1b) but also in each individual month considered (Figure 3, left column). While negative

341 and positive TST anomalies (i.e., negative and positive deviations from the long-term monthly mean) are almost

342 uniformly distributed for SSN values smaller than the SC14 maximum (blue dotted lines), an increase in the solar

343 forcing exceeding the SC14 SSN maximum leads to a higher probability of positive TST anomalies. The strength of

344 the correlations changes over the season, such that a stronger connection between the solar forcing and the temperature

345 response at the tropical stratopause is given in late autumn (November: r=0.28) and late winter (February: r=0.34;

346 March: r=0.42). In these months, a particular strong solar forcing (indicated by the SSN value of the SC19 maximum

347 (red dotted lines)) is almost always associated with a positive temperature anomaly at the tropical stratopause. Weaker

348 correlations and a broader distribution of negative and positive temperature anomalies, even during periods with

349 especially pronounced solar activity, are calculated for the midwinter season (December: r=0.15; January: r=0.16).

350 These findings are consistent with an increase in the overall variability in the TST during December and January,

351 making it more difficult for the relatively weak solar induced signals to be distinguished from the background noise.

352 The higher variability in the TST during December and January is probably a result of the higher variability of the

353 tropical branch of the Brewer-Dobson circulation (BDC) in boreal winter (e.g., Butchart, 2014).

354 According to the general concept of the "top-down" mechanism the initial signal in the TST would be accompanied

355 by a strengthening of the PNJ via a modification of the meridional temperature gradients. Considering the statistically

356 significant temperature signals and correlations at the tropical stratopause in the MPI-ESM-HR model (Figure 3, left

357 column), we expect a dynamical response of the PNJ in our simulations. However, the correlations between the SSN

358 and the PNJ time series (Figure 3, middle column) do not show statistically meaningful relations between the solar

359 forcing and the dynamical response of the PNJ. Only during February, a weak but statistically significant correlation

360 is found, which might be related to the enhanced impact of the solar forcing in the TST during the same month.

361 However, this connection as well becomes insignificant, if the correlations are calculated based on the unfiltered SSN

362 and PNJ time series. Figure 3 (right column) shows the correlations between the solar forcing and the zonal mean

363 zonal wind for the lower (and more northward) 10 hPa anomaly time series. We find the strongest (and significant)

364 correlations in November (r=0.25) and December (r=0.13), although these correlations become (again) negligible if

365 the correlations are calculated based on unfiltered model data. The differences in the timing between the maximum

366 correlations of the SSN with the PNJ (February) and the 10 hPa zonal wind time series (November and December) are

hat gelöscht:
hat gelöscht:
hat gelöscht:
hat gelöscht:

371 not in line with the established idea of a successive "poleward and downward" progression of the dynamical solar

372 signal. Furthermore, the computed SSN/PNJ correlations for November, December, January and March are ≤ 0.06,

373 implying that the characteristics of the PNJ are not markedly influenced by the magnitude of the solar forcing and thus

374 the amplitude of the solar cycle.

375
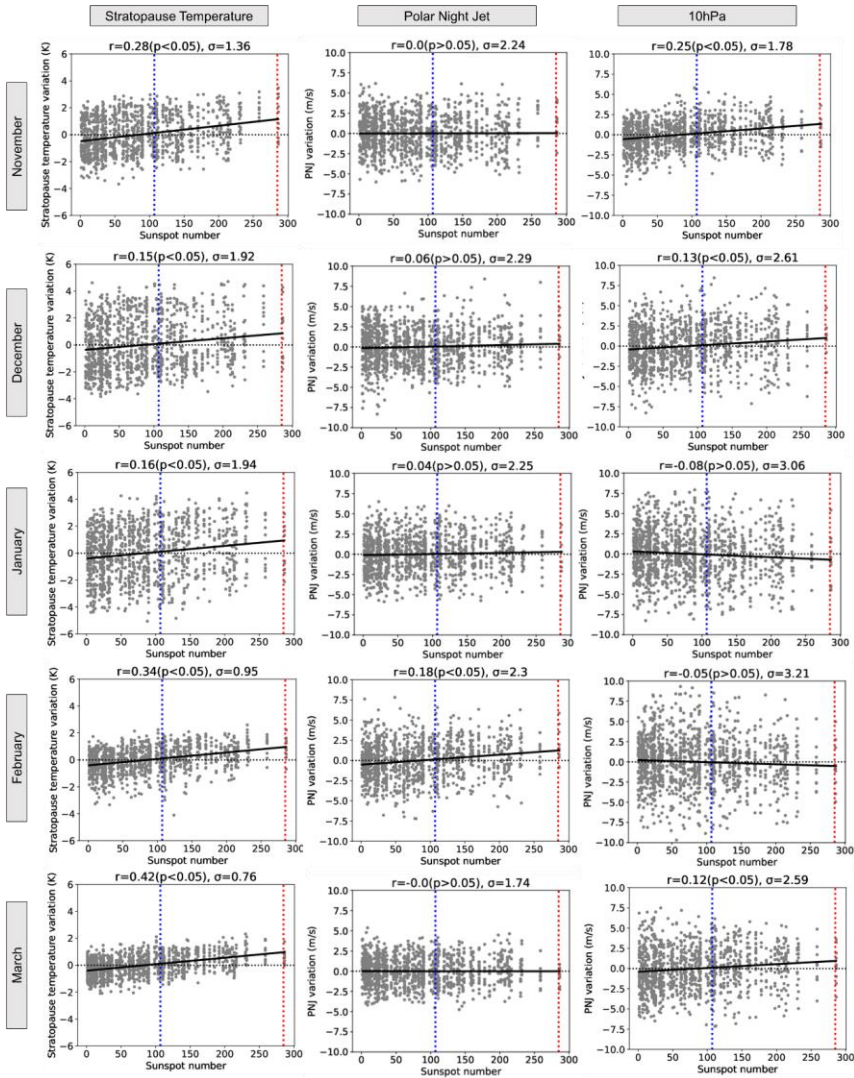
Figure 3: Scatter diagram of the stratopause temperature (left column), PNJ (middle column) and zonal-mean zonal wind averaged over 55°N – 65°N at 10 hPa (right column) variations vs. SSN. The numbers given in the headings show the correlation coefficients (r), their statistical significance (p < 0.05: significant correlation, or p > 0.05: insignificant correlation), and the overall variation (σ). The dotted blue and red lines indicate the SSN at solar cycle maximum for SC14 and SC19 (the weakest/strongest solar cycles considered in the simulations).

381

382

Figure 3 demonstrates that while the connection between the solar forcing and the TST is clearly visible in our correlation analysis, the potential dynamical response in the NH is harder to detect, especially due to the highly variable polar vortex. Therefore, we proceed using a MLR analysis to separate the potential dynamical solar induced signals from other internal generated disturbances in the ensemble mean.

After having analyzed the variability of the TST, the PNJ and the 10 hPa zonal-mean zonal wind, we will now isolate potential solar signals by the aid of MLR. Figure 4 shows the solar regression coefficients, scaled to a mean amplitude of the solar cycle (180 SSN), for the zonal-mean temperature (top row), the zonal-mean zonal wind (middle row) and the EPF (vectors) and its divergence EPFD (colors) (bottom row) for each NH winter month (November – March). Here, we focus on the potential solar cycle signals between the equator and the North Pole and pressure heights in 1.000 hPa – 0.1 hPa for the temperature and wind responses and 100 hPa – 0.1 hPa for the EPF diagnostics. We find a significant response in the zonal mean temperature at the tropical stratopause (Figure 4, top row) with a maximum response at the equator of 1.2 K during November. The solar induced temperature signal is confined to the inner tropics in late autumn and early winter and advances towards higher latitudes between January and March. This is consistent with the seasonal march of the incidence angle of solar radiation after the winter solstice in December. In the middle to polar latitudes, we find a clear dipole in the temperature anomalies especially during November and December. This dipole is characterized by distinct (and significant) positive temperature anomalies in the lower mesosphere and upper stratosphere and weak (and insignificant) negative anomalies in the middle and lower stratosphere. Particularly the pronounced polar heating in the upper stratosphere from November to December agrees well with a most recent analysis of ERA-interim reanalysis data by Kuroda et al., (2022). The detected temperature signals in the middle atmosphere in November and December are in line with the anomalies in the zonal-mean zonal wind (Figure 4, middle row), which indicate a stronger (and thus cooler) polar vortex during these months. Additionally, a convergence of the EPF (indicated by the reddish colors in Figure 4, bottom row) and its (here downward oriented) vectors imply a reduced upward propagation of planetary waves due to the strengthening of the polar vortex. The maximum (and significant) response in the stratospheric zonal-mean zonal wind in the area of the polar vortex, is located at ~60°N at 10 hPa. Here, we find positive anomalies of the zonal-mean zonal wind of ~1 m/s. Given the mean zonal-wind speeds between 20 m/s (November) and 30 m/s (December), simulated by the model (not shown) at this height and latitude, the solar influence seems rather small in comparison. The detected dipole in the zonal-mean temperature starts to weaken from January on and vanishes almost completely until March. During the same months, we find a (yet insignificant)

weakening of the polar vortex which allows for more upward propagation of planetary waves (indicated by a divergence of the EPF (bluish colors) and upward oriented vectors). In the troposphere, a weak (≤ 0.5 m/s) but significant westerly wind anomaly around ~60°N can be detected in November and December. The weak tropospheric wind response agrees with other studies (Matthes et al., 2006; Schmidt et al., 2010; Ineson et al., 2011; Chiodo et al., 2012; Langematz et al., 2013; Kuroda et al., 2022; Drews et al., 2022).

While in some studies the march of the westerly wind anomalies from the middle atmosphere to the surface seems to follow the proposed "poleward and downward" concept (e.g., Matthes et al., 2006; Ineson et al., 2011; Drews et al., 2022), the signal transmission in the MPI-ESM-HR and other model simulations (e.g., Schmidt et al., 2010; Chiodo et al., 2012; Kuroda et al., 2022) rather follows a "downward-only" storyline. Additionally, the description of the westerly wind anomalies at the surface is sometimes inconsistent with the idea of a successive downward propagation of the signal from higher to lower altitudes. As an example, significant westerly wind anomalies at the surface at middle latitudes are already present in November in the modeling studies of Matthes et al. (2006) and Kuroda et al. (2022), even though the major signal is still high up in the middle atmosphere. Furthermore, in Kuroda et al. (2022) the westerly wind anomalies at the surface at middle latitudes are present throughout the complete season (i.e., in all months between November-March), similar to our MPI-ESM-HR simulations. In other studies, the westerly anomalies are insignificant (e.g., Schmidt et al., 2010) or do not reach the ground (e.g., Chiodo et al., 2012). This implies that the detected surface wind anomalies could be independent from the seasonal march in the middle atmosphere and might rather be a product of the internal variability in the troposphere (i.e., the AO or NAO) itself. Likewise, the temperature response to the solar cycle in the troposphere with positive temperature anomalies of ≤ 0.2 K at the surface is rather weak (Figure 4, top row). Interestingly, these small temperature signals are significant in the tropics in all considered months, which is consistent with the high (and relatively constant) solar insolation in the inner tropics and a damped overall variability compared to the extratropical regions. By contrast, the significant surface temperature anomalies in the extratropical regions are located between 50°N and 60°N until January and shift towards the polar latitudes in February and March.

442
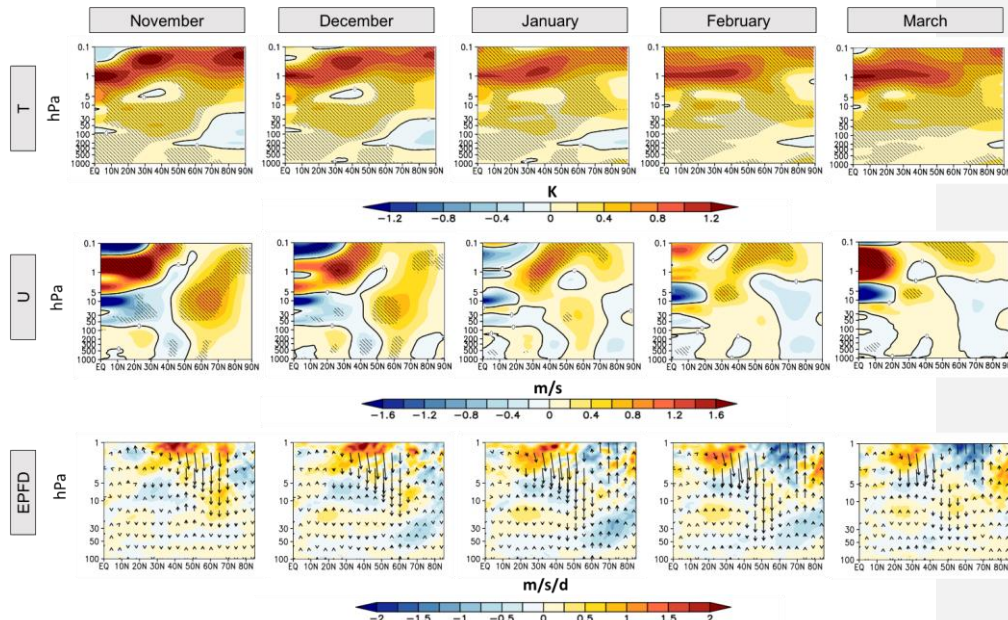
Figure 4: The ensemble mean long-term response (based on MLR) to the solar cycle of the zonal-mean temperature (first row), zonal-mean zonal wind (second row) (hatched regions mark 95% statistical significance), and the EPF (vectors) and the divergence of the EPF (EPFD, colors) in the NH during the boreal winter season. All results have been scaled to 180 SSN.

447

448

So far, we focussed on the discussion of the potential solar signals in the ensemble mean derived from the 10 individual

MiKlip historical simulations thus obtaining statistically more robust results than is possible through analyses of single

simulations. The necessity of working with ensemble mean results is impressively demonstrated by comparing two of

our 10 individual ensemble members. Figure 5 shows the solar regression coefficients for the zonal-mean temperature

and zonal-mean zonal wind for the ensemble members 1 (EM1, top panel) and 4 (EM4, bottom panel), as in Figure 4.

The derived patterns for the solar zonal-mean temperature signal in EM1 show distinct similarities with the ensemble

mean. As an example, we find a (significant) maximum temperature response around the tropical stratopause.

Furthermore, the distribution of the temperature anomalies in the middle to higher latitudes again displays the polar

heating in the lower mesosphere and the upper stratosphere and the cooling in the middle to lower stratosphere. Again,

this pattern starts to weaken from January on. We notice that in comparison to the ensemble mean, fewer areas depict

461 significant temperature signals, even though the magnitude of the temperature response is stronger. This can be

462 attributed to the fact that the analysis only includes 120 model years and thus ~12 solar cycles (instead of 1.200 and

463 ~120 in the ensemble mean), which is seemingly not enough to dampen the internal variability and inhibits the solar

464 induced signals to become significant against the overall background noise. Likewise, the solar response of the zonal-

465 mean zonal wind in the middle atmosphere in EM1 shows the main characteristics, as already noticed in the ensemble

466 mean, such as a strengthening of the polar vortex in November and December and a subsequent weakening and a

467 conversion in sign afterwards. However, none of the detected signals in the area of the polar vortex are statistically

468 significant. As for the response of the zonal-mean zonal wind at the surface, we detect significant anomalies in January

469 and February. The geographical distribution of the anomalies (westerly wind anomalies at middle latitudes and easterly

470 wind anomalies at polar latitudes), however, mimic a negative phase of the AO which is not in line with the general

471 concept of solar induced "top-down" influences.

472 In EM4, the initial temperature signal in the upper tropical stratosphere is, as in EM1, visible throughout the complete

473 season and the strongest in November and December. Thus, the response to the solar cycle in these latitudes and

474 heights turns out to be a robust feature in the MPI-ESM-HR model experiments. However, even though exactly the

475 same solar forcing has been applied in EM4 as in EM1, the initial temperature signal is not significant (most likely

476 due to the individual internal variability in this ensemble member) and the dynamical response of EM4 in the

477 extratropical regions looks very different. For instance, we find a cooling of the polar upper stratosphere and a

478 (significant) warming in the middle to lower stratosphere in December and January. This pattern is common during

479 SSWs, which (by chance) could have been more frequent in EM4 during December and January than in EM1. The

480 strong and significant easterly wind anomalies in the middle atmosphere, indicating a slowdown of the polar vortex

481 during these months, underpin this hypothesis. These findings imply that the detected signals in EM1 could also be a

482 result of (by chance) less frequent SSWs in EM1 leading to a potentially misleading attribution to solar variability. In

483 our simulations, four out of 10 simulations show a weakening of the polar vortex during high solar activity, while six

484 depict a strengthening of the latter, which may explain the rather weak tendency to westerly wind anomalies in the

485 ensemble mean.

486 Either way, our results point to the fact that the internal dynamics of the polar vortex have the ability to control the

487 transmission of potential solar induced signals from the tropics to the polar regions and are thus more important than

488 the amplitudes of individual solar cycles (compare also Figure 3), as recently claimed by Drews et al. (2022).

hat gelöscht: .

hat gelöscht: ,

hat gelöscht: .

492

493
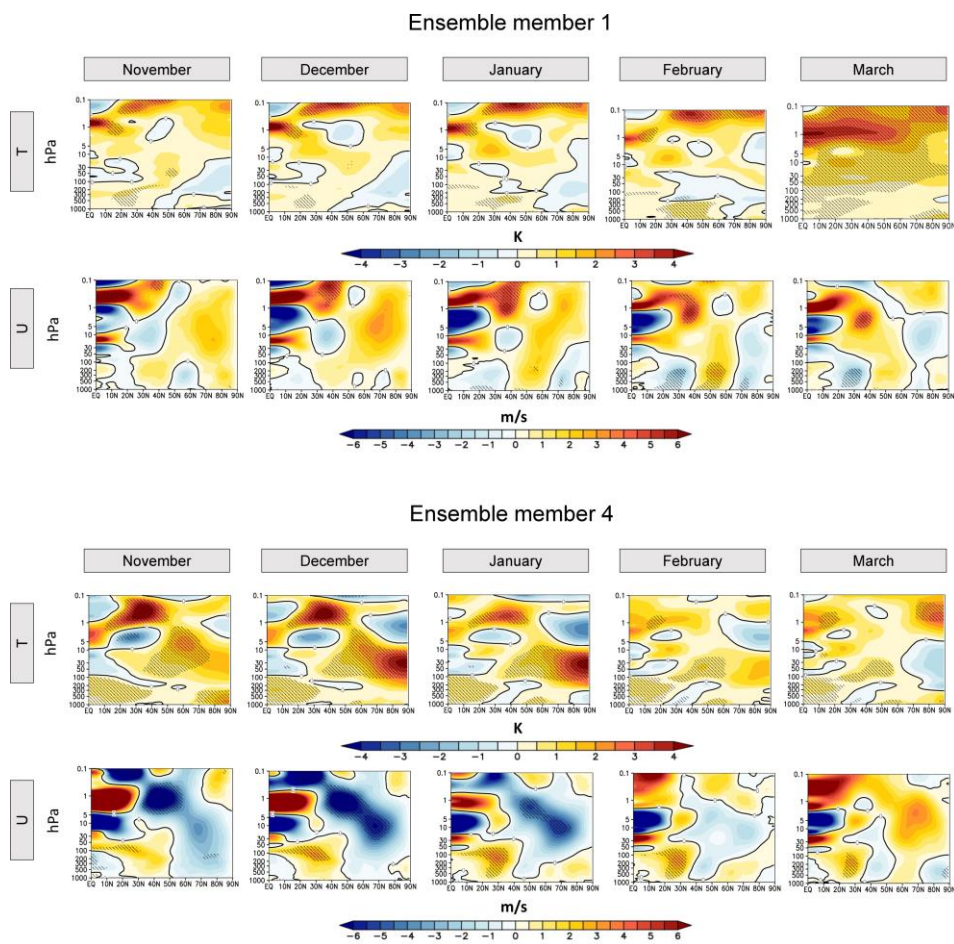
Figure 5: Long-term response (based on MLR) to the solar cycle of the zonal-mean temperature (first row) and the zonal-mean zonal wind (second row) (hatched regions mark 95% statistical significance) in the two ensemble members EM1 (top panels) and EM4 (bottom panels) in the NH during the boreal winter season. All results have been scaled to 180 SSN.

499

500

5. Direct and lagged surface solar signals

Our results so far indicate a robust response of the TST to the quasi-decadal solar cycle. The subsequent dynamical response in the NH during the boreal winter season, however, is difficult to assess. By the aid of a MLR analysis we could detect weak solar cycle imprints in the zonal-mean temperature and the zonal-mean zonal wind in the ensemble mean. However, these signals are not robust among all individual ensemble members, especially with respect to the detected anomalies in the zonal-mean zonal wind at the surface which seem to be independent of the signals in the middle atmosphere.

510 Nevertheless, in the next step, we first aim at detecting potential solar signals at the surface by applying the MLR

511 analysis to mean sea level pressure (MSLP) data in NH winter. Figure 6 shows the monthly solar regression

512 coefficients for MSLP, scaled to a mean solar cycle amplitude of 180 SSN, in the HadSLP2 observational dataset

513 (Allan and Ansell, 2006) for the same period as simulated (1880 – 1999). In order to check for eventual time lags

514 between the applied solar forcing and the model response, as suggested for example by Gray et al. (2013), lagged

515 regressions were calculated by shifting the solar predictor time series against the observations so that it leads the model

516 data between one and four years. Our results show positive and negative anomalies in the MSLP in the middle and

517 polar latitudes which mimic positive and negative phases of the AO in a rather random than systematic way. As an

518 example, we find an AO-positive like pattern (i.e., negative pressure anomalies over the North Pole and positive

519 pressure anomalies in the surrounding middle latitudes) in November at lag year four, in December at lag year four,

520 in February at the lag years one to three and in March at lag year one. The most pronounced AO-positive anomalies,

521 with a negative but insignificant anomaly of ~2 hPa over the North Pole and a positive anomaly of the same magnitude

522 in the middle latitudes, are given at lag year 2. Hence, the strength of the detected potential solar signals in our

523 HadSLP2 analysis is in line with other studies assessing observational products (e.g., Gray et al., 2013; Kuroda et al.,

524 2022; Drews et al., 2022). The detected maximum impact at lag year 2 in February in our analysis, however, agrees

525 with Kuroda et al. (2022) and Drews et al. (2022) but differs from Gray et al. (2013) who found a maximum response

526 at lag year 4 in the DJF mean. These discrepancies in the timing of the peak solar-induced surface signal in the HadSLP

527 MSLP data can only be explained by differences in the analysis techniques, and reveal a high sensitivity of solar-

528 induced surface signals to the applied methodology and individual interpretation of the results. Furthermore, and due

529 to the lack of data covering the whole atmospheric domain over the complete historical period, it is not possible to

530 connect the potential surface solar signals to the seasonality in the middle atmosphere. This applies to our and the

531 original studies (e.g., Gray et al., 2013).
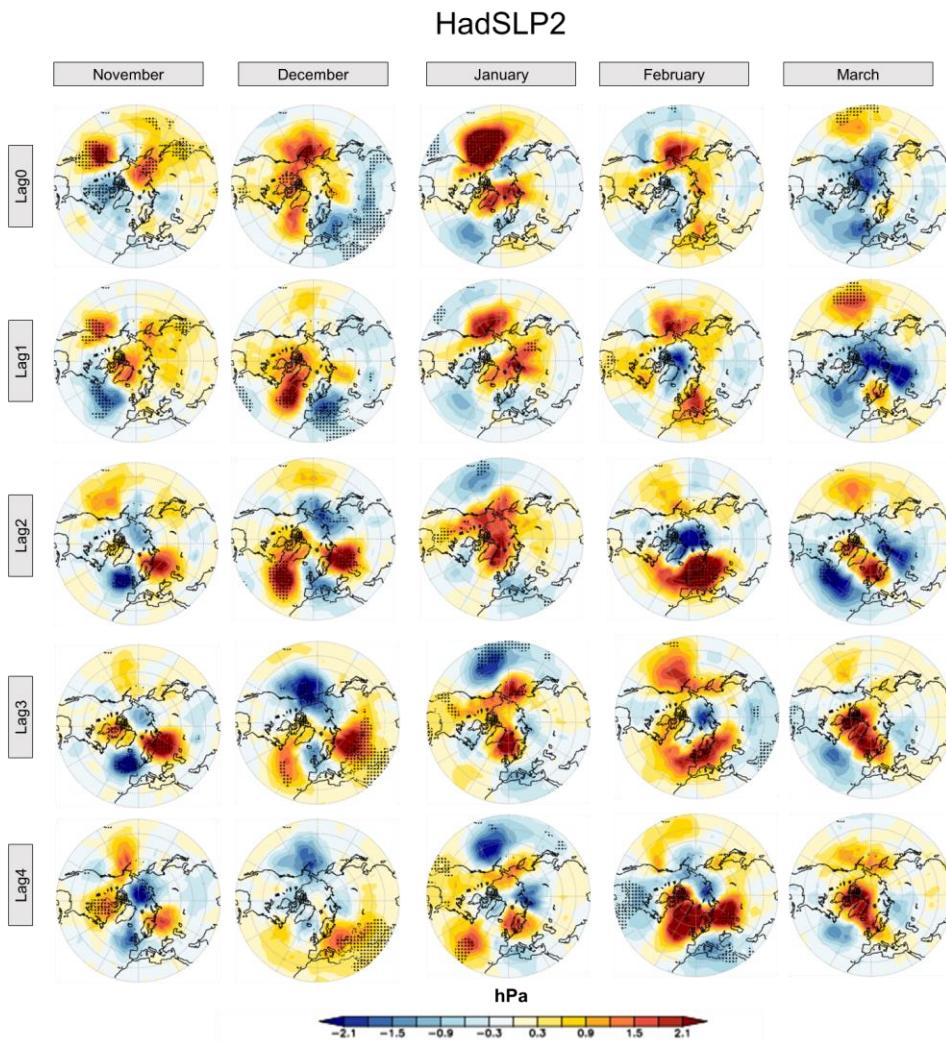
HadSLP2

Figure 6: The (lagged) response of mean sea level pressure (MSLP) to the solar cycle in the NH during the boreal winter season for the HadSLP2 dataset (dotted regions mark 95% statistical significance). Columns denote the individual months of the winter season; rows indicate the lag of the MSLP time series with respect to the solar forcing time series.

532

533
534
535
536

537

hat gelöscht: the

hat gelöscht: level of significance

Figure 7 shows the same analysis for the MiKlip historical simulations, i.e. the ensemble mean of the solar regression coefficients for the MSLP for each month (November to March) and the (lag) years zero to four. We detect AO-positive-like anomalies in the MSLP in December at the lag years 0 and 1, in January at the lag years 0 to 4 and in February at the lag years zero to four. The strongest negative MSLP anomalies over the North Pole show a response of ~ -1.5 hPa and ~ +1.5 hPa in the middle latitudes in January and December. Thus, the overall model response is weaker compared to the observational data. This is not surprising given the fact that the model results depict the mean over 10 ensemble members (with respective dampening effects) compared to one 'ensemble member' representing the observations. While the detected magnitudes of the MSLP anomalies in MPI-ESM-HR agree with other solar cycle model studies (e.g. Gray et., 2013; Scaife et al., 2013; Andrews et al., 2015; Drews et al., 2022), the detected timing (i.e. the progression of the signals from the middle atmosphere to the surface) in the MPI-ESM-HR does not fit the narrative of the "top-down" mechanism as described most recently by Kuroda et al. (2022) and Drews et al. (2022). In these studies, the authors find the most pronounced AO-positive like pattern in February at the surface and link this to the coupling between the stratosphere and the troposphere, which peaks in exactly this month. In contrast, in our model simulations the strongest coupling between the stratosphere and the troposphere appears in December (see Figure 4), while the most pronounced AO-positive like patterns appear in January and February at different lag years. Statistical studies based on MLR analysis of observed and reconstructed MSLP data find both NAO signals in early and late winter at different lags (Grey et al., 2016; Ma et al., 2018). We, therefore conclude that the detected surface solar signals could rather be a product of the internal variability in the troposphere itself than being necessarily a consequence of the proposed "top-down" mechanism. Even if we assume that the detected surface signals have a pure solar source (and the "top-down" mechanism is always present during solar maximum years) it seems to be questionable in our view if these tiny signals would have the capability to synchronize powerful large-scale climate modes such as the AO or the NAO, if they only emerge once per decade over the duration of a month. As an example, the Icelandic Low and the Azores High, both controlling the pressure gradients in the North Atlantic sector, show a month-by-month variation of ~8.5 hPa and ~6 hPa during winter time in the model (not shown).
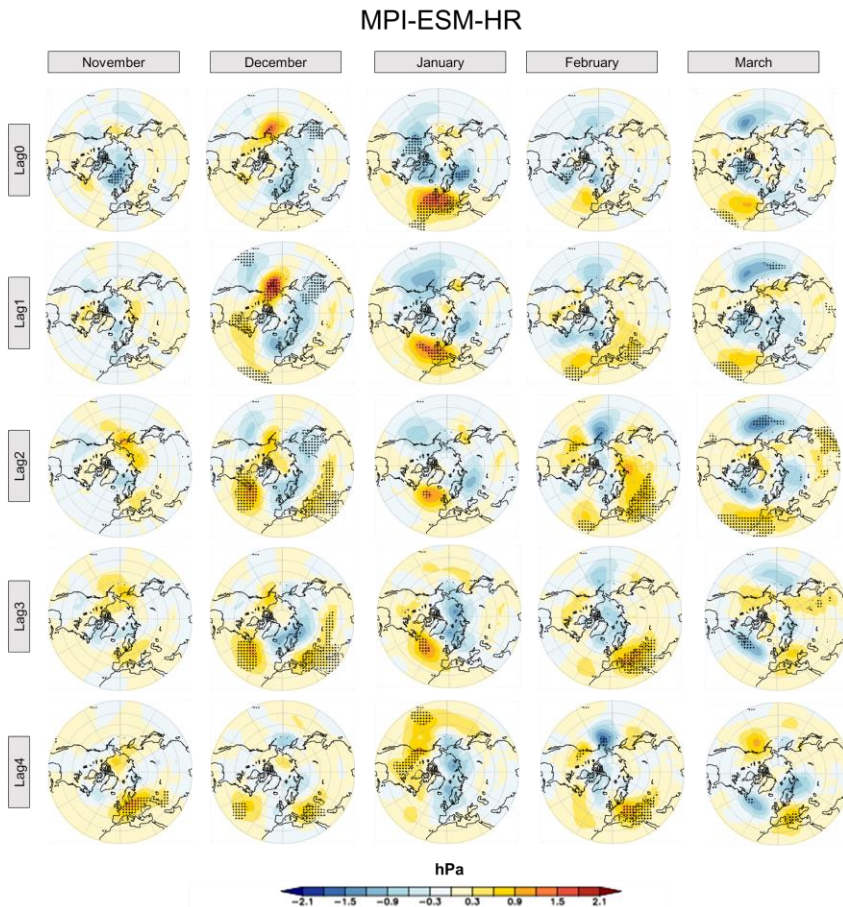
MPI-ESM-HR

568

569   **Figure 7:** As Figure 6, but for the ensemble mean of the MPI-ESM-HR MiKlip historical simulations.

570

571   **6 A synchronization of the NAO by the solar cycle?**

572   In the following, we will address the question, if the quasi-decadal variations of the solar cycle have the ability to

573   synchronize the decadal component of the NAO, as proposed by Thiéblemont et al., (2015) and Drews et al., (2022).

574   For a better comparison, we apply the same analytical strategy as proposed by Thiéblemont et al. (2015) to our model

575   simulations and the HadSLP2 data, however with the exception that we use the SSN instead of the F10.7 solar flux

576 times series as a solar proxy. Since both the SSN and F10.7 time series show the same oscillations on the interannual

577 and decadal timescale, this is irrelevant for the interpretation of the results. First, an EOF analysis is applied to the

578 deseasonalized MSLP data over the Atlantic sector (20 – 80°N, 90°W – 40°E) in the winter season (DJF averaged).

579 Before continuing, we compared the spatial pattern of the EOF1 between the modelled and observed data and found

580 good agreement with respect to the centers of action and overall characteristics (not shown). The resulting leading

581 principal components (PC1) are then used to describe the variability of the NAO. To mute major parts of the

582 interannual variability, we apply a Butterworth bandpass filter with cutoff frequencies of 9 and 13 years to the PC1

583 and the SSN time series. As a result, the filtered PC1 and SSN time series only include the oscillations operating on

584 the quasi-decadal timescale. Subsequently, lead/lag correlations are calculated between the bandpass-filtered PC1 and

585 SSN timeseries for both the complete dataset and all individual ensemble members (1 to 10). Drews et al. (2022)

586 recently argued that the correlations would become more meaningful during the course of the 20th century due to a

587 series of solar cycles with stronger amplitudes. We, therefore, compute the correlations for three different time

588 segments: the whole period (WP) (1880 – 1999), the early period (EP) with weaker solar amplitudes (1880 – 1940)

589 and the late period (LP) with more pronounced solar amplitudes (1941 – 1999).

590 For the HadSLP2 dataset (Figure 8, left column/first row) positive correlations between the decadal variation of the

591 NAO and the solar forcing is found for the lag years one to four in both the WP and the LP periods, with maximum

592 correlations at lag year three during the LP. For the EP, we find an out-of-phase relation between the solar time series

593 and the NAO on the decadal timescale. The evaluation of this (1 ensemble member) observational dataset implies that

594 the solar forcing actually leads the surface response by a couple of years and that this relation is more pronounced

595 during phases of higher solar activity. Indeed, similar phase relations in the different time segments are given in

596 individual ensemble members of the MiKlip historical simulations (e.g., EM9 (Figure 8, left column/sixth row).

597 However, phase relations like these seem far from being a robust feature if all model runs are considered. As an

598 example, EM5 (Figure 8, left column/third row) indicates positive correlations between the decadal behavior of the

599 SSN and the NAO time series for the lag years one to three during the EP, while this relation reverses (showing

600 negative correlations) during the WP and LP. This is also true for EM3 (left column/third row) and EM7 (left

601 column/fifth row). Other ensemble members (EM2; Figure 8, right column/second row) suggest a maximization of the

602 solar impact at lag year zero and this independently of the considered period. Furthermore, EM6 (Figure 8, right

603 column/fourth row) indicates stronger positive correlations at positive lag years during the EP than during the LP. The

605 most striking discrepancies, however, come from EM1 (Figure 8, left column/second row) and EM4 (Figure 8, right

606 column/third row). While EM1 shows negative correlations between the solar forcing and the NAO at positive lags

607 (in all time segments), this is vice versa in EM4. These surface responses in EM1 and EM4 are, however, opposite to

608 what would be expected from the polar vortex responses in these two ensemble members (a pronounced strengthening

609 of the polar vortex and a downward propagation of westerly wind anomalies to the surface in EM1, and a weakening

610 of the polar vortex and a downward propagation of easterly wind anomalies to the surface in EM4 during winter (see

611 Figure 5)) and opposite to the 'top-down mechanism'.

612 When applied to the complete dataset of the MiKlip historical simulations, the correlation analysis yields a weak

613 positive (albeit significant) correlation at the lag years two to four, rather independently of the considered time

614 segment. This, however, should rather be interpreted as a slight (and by chance) overhang to positive correlations in

615 the MiKlip dataset (that could change in a larger ensemble) than a robust physical connection between the solar forcing

616 and the NAO. To verify whether the use of the seasonal mean (DJF) might dampen the solar cycle response, as

617 discussed by Drews et al. (2022), we repeated the analysis for the individual winter months (December, January and

618 February, see Supplementary Figure 2) for the model data. We did not detect stronger connections between the decadal

619 solar forcing and the NAO in the calculations based on individual months compared to the seasonal mean. On the

620 contrary, the correlation analysis based on the December months (i.e., the month where we find the "strongest" "top-

621 down" signals in the middle atmosphere) depicts negative correlations at positive lag years. In summary, given all of

622 these inconsistencies we suspect that there is no robust connection between the quasi-decadal solar oscillations and

623 the respective phase of the NAO in the CMIP5 MiKlip historical ensemble simulations.

hat gelöscht: materia
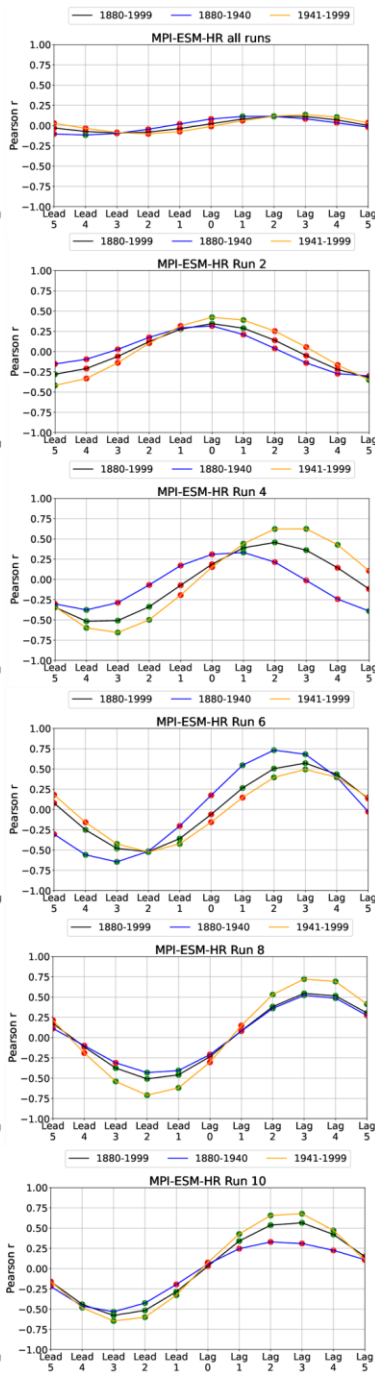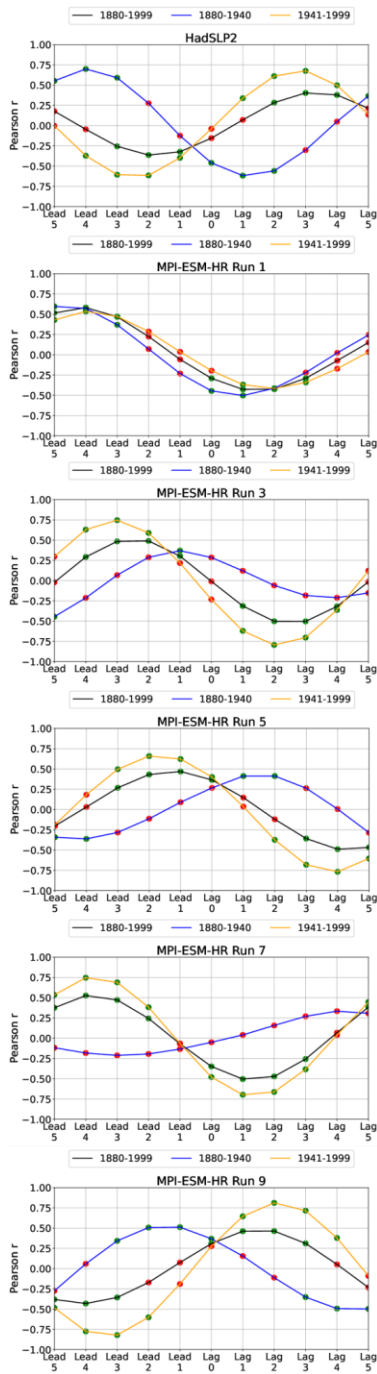
Figure 8: Lead/lag-correlations between the seasonal mean (DJF) bandpass filtered PC1 based on NAO and SSN time series. For the HadSLP2 dataset and the ensemble mean of the MPI-ESM-HR historical simulations (top row) and the individual MPI-ESM-HR historical runs (rows 2 to 6) for different periods. Green dots mark statistically significant (95%) correlations.

hat gelöscht: over

7. Summary and discussion

Our analysis of the MiKlip historical ensemble simulations, conducted with the state-of-the-art Earth system model MPI-ESM-HR, revealed robust (and statistically significant) solar signals in the TST (see Figures 1 and 2). The dynamical response to the initial solar temperature signal at the tropical stratopause, in the NH middle to polar latitudes during the boreal winter season, however, showed a large spread among our data. This applies to the variability of the PNJ and the 10 hPa zonal-mean zonal wind time series, which both did not show meaningful correlations with the solar forcing (see Figure 3). When removing other than decadal variability components by MLR analysis, we were able to detect (albeit rather weak) solar signals in the NH winter, in both the ensemble mean zonal-mean temperature and zonal-mean zonal wind, that basically agree with the proposed "top-down" influence of solar variability in the middle atmosphere (see Figure 4). However, the MLR analysis based on individual ensemble members revealed signals of opposite direction (i.e., a strengthening (EM1) or weakening (EM4) of the polar vortex during periods of high solar activity) (see Figure 5). Furthermore, we find indications that the detected anomalies in the zonal-mean zonal wind at the surface are most likely independent of the signals in the middle atmosphere. The alleged surface solar signals in MSLP seem to mimic AO-positive (and AO-negative) patterns rather randomly than in a systematic way. This applies to the HadSLP2 data (Figure 6) and to the model data (Figure 7), which both depict most pronounced an AO-positive pattern in January and February at different lag years however in months, where the strong stratospheric influence (in December) is already weak or even reverses sign in the model (compare Figure 4). With respect to the suggested synchronization between the decadal solar forcing and the NAO (e.g., Thiéblemont et al., 2015) we cannot find any meaningful relations in the MiKlip historical simulations. This is supported by the fact that all ensemble members show very individual phase relations (i.e., positive/negative correlations and maximizations during different lag years) between the solar and the NAO time series. Additionally, more robust correlations could not be achieved in different time segments (i.e., periods with stronger or weaker solar forcing). These findings apply to the seasonal winter mean (DJF) as well as to individual winter months (December, January and February). As a

hat gelöscht: and thus

658 consequence, the detected phase relations in the HadSLP2 dataset should be interpreted carefully with respect to

659 potential physical connections between the solar forcing and the NAO, in particular since the observations represent

660 only one single ensemble member.

661 In summary, we draw four major conclusions:

662   1. The decadal variations of the TST in the MiKlip historical simulations are a product of the 11-year solar

663   cycle. In the course of this, an increase in the solar intensity leads to enhanced radiative shortwave heating

664   rates and a warming of the TST. These findings are consistent with other modeling studies concerning the

665   imprints of the 11-year solar cycle in the tropical upper stratosphere (Matthes et al., 2004, 2006; Schmidt et

666   al., 2010; Ineson et al., 2011; Chiodo et al., 2012; Langematz et al., 2013). The solar signals in the TST are

667   statistically significant and robust and were detected by our correlation and MLR analyses.

668   2. The dynamical response of the NH during winter in the middle atmosphere shows a weak strengthening of

669   the polar vortex during solar maximum in the ensemble mean in the MLR analysis. However, the signals

670   (especially in the zonal-mean zonal wind) are mostly insignificant and of opposite sign in individual ensemble

671   members, and thus not a robust feature. We suppose that the dynamical background state in the middle

672   atmosphere (i.e., the variability of the polar vortex) seems to play an important role for the transfer of the

673   initial radiative solar signal from the upper tropical stratosphere down to the troposphere in NH winter. The

674   important role of middle atmosphere dynamics in modulating potential solar signals is currently investigated

675   as part of the SOLCHECK project and will be published in a subsequent paper (Wenjuan Huo, personal

676   communication).

hat gelöscht: . They

hat gelöscht:

679   3. The detected anomalies in the zonal-mean zonal wind and MSLP at the surface seem not to be related to the

680   timing of the seasonal march of the signals in the middle atmosphere and are most likely a manifestation of

681   the internal variability in the troposphere itself.

682   4. Concerning the decadal variations of the NAO and the solar forcing, our results suggest that both are

683   independent from each other. We find a range of phase relations between the NAO and the solar forcing

684   throughout our ensemble members, which implies a random statistical relation rather than a physical sound

685   connection.

686

687   It should be noted that we did not explicitly analyze a potential TSI controlled bottom-up effect on the solar surface

688   signal, as bottom-up effects are rather confined to tropical latitudes with a prolonged influence of the TSI throughout

689   the year (e.g., Meehl et al., 2008). Moreover, potential effects related to energetic particle precipitation are not

690   explicitly included in the MiKlip experiments. Since these effects are known to be rather small and even less

691   understood than the 11-year solar cycle surface imprints, we don't think they would alter our results significantly

692   (please see the introduction section).

693   Since the critical study of Chiodo et al. (2019), the "top-down" mechanism and its surface imprints have been further

694   discussed in the scientific community. It is unquestionable that early studies with GCMs and CCMs found evidence

695   of a "top-down" mechanism in the middle atmosphere which in most cases penetrated into the troposphere in NH

696   winter (Matthes et al., 2004, 2006; Schmidt et al., 2010; Ineson et al., 2011; Chiodo et al., 2012; Langematz et al.,

697   2013). These studies all reproduced more or less the basic features of the "top-down" mechanism, thus confirming the

698   physical mechanisms at work suggested by Kodera and Kodera (2002). In contrast, more recent simulations with

699   CCMs and ESMs do not seem to find statistical responses of surface variables to the decadal solar forcing (e.g., Chiodo

700   et al., 2019; this study). Only Drews et al. (2022) showed a near-surface solar imprint for solar cycles with strong

701   amplitudes. The MiKlip simulations are more in line with Chiodo et al. (2019), who argued that the alleged surface

702   solar signals could be an incidental product which is only detectable during phases with stronger solar cycles. Our

703   results even suggest that robust solar surface imprints are basically absent throughout the complete historical period

704   and are thus not sensitive to the amplitude of individual solar cycles. At this point we would like to emphasize that in

hat gelöscht: time series

hat gelöscht: In this context we

hat gelöscht: manifold

hat gelöscht: all of

hat gelöscht: by chance

hat gelöscht: but not

hat gelöscht: ,

hat gelöscht: se

hat gelöscht: We assume that including these effects would not significantly affect the simulated solar surface signal.

715 contrast to previous studies, the MiKlip simulations represent a transient climate system driven by a realistic (observed)
716 solar forcing thus enhancing the confidence in a comparison of our model results to observations.
717 We suggest that the gradual 'fading away' of significant solar near-surface signatures in more up-to-date model studies
718 is closely related to progresses made in model development and computer capacities allowing for ensemble
719 simulations. The early simulations were conducted with fixed lower boundary conditions (i.e., prescribed SSTs from
720 observations or control run experiments) (Matthes et al., 2006; Schmidt et al., 2010; Chiodo et al., 2012). Some applied
721 perpetual conditions for the solar forcing (i.e., perpetual solar maximum vs. perpetual solar minimum) and steady-
722 state conditions for the greenhouse gas forcing (Matthes et al., 2006; Schmidt et al., 2010; Ineson et al., 2011). While
723 these models included the necessary physical mechanisms, i.e., UV radiation codes and middle atmosphere dynamics,
724 to capture the solar UV-induced top-down solar signal, the complex nature of physical and chemical processes and the
725 spectrum of internal variability were reduced. Prescribed SSTs, for example, prevent the model from developing the
726 complete spectrum of interannual variability in the troposphere (e.g., induced by the internal variability of the NAO),
727 which might counteract potential surface solar signals. In addition, steady-state background conditions in atmospheric
728 greenhouse gas concentrations and prescribed ozone depleting substances do not take into account transient adjustment
729 processes in the atmospheric dynamics, which again lead to a reduction of the overall internal variability and maybe
730 an overestimation of solar-induced signals. Moreover, due to more limited computer capacities, the results from the
731 early model studies were mostly based on single simulations.
732 In contrast, our results show that in a state-of-the-art climate model system the potential solar near-surface signals are
733 rather weak, not robust and inconsistent with the timing in the middle atmosphere. One potential reason is the
734 additional variability component introduced into the model by the interactively coupled ocean model. Misios and
735 Schmidt (2012) also showed the impact of an interactive ocean on the simulated solar response in the tropical Pacific
736 region. While individual ensemble simulations produce the expected phase correlation between the NAO and the solar
737 cycle, others show the opposite behavior. Thus, we do not find any convincing evidence in our model simulations of
738 the alleged decadal synchronization between the NAO and the solar forcing, as suggested by Thiéblemont et al. (2015).
739 In our view, the decadal near-surface signals detected in the MiKlip historical simulations are a product of the internal
740 variability in the troposphere itself and not a physical consequence of the "top-down" mechanism.
741 We would further like to mention that a strong reduction of the interannual variability in two basically independent
742 time series – be it by bandpass filtering like in our study or in Thiéblemont et al. (2015), or by using wide running

hat gelöscht: Marsh et al., 2007;

hat gelöscht: Marsh et al., 2007;

hat gelöscht: disposed

hat gelöscht: of

hat gelöscht: In both cases,

hat gelöscht: is damped

hat gelöscht: mean

hat gelöscht: We, thus,

751   mean windows like in Drews et al. (2022) – will always lead to significant alignments of these two time series at some

752   point, if they are shifted towards each other gradually. Thus, the phase relations in our (and other studies) seem to be

753   a statistical artifact and not the consequence of a physical phase coupling. We also would like to question if the oceanic

754   memory is sensitive enough to store the tiny surface solar signals (even if there are some) for the duration of a complete

755   decade. Hence, in our opinion a much more profound solar forcing would be needed to significantly influence the

756   ocean temperature and thus dynamically driven feedbacks. Such forcings, however, typically operate on the centennial

757   timescale which is characterized by phases of Grands Solar Maxima and Minima (e.g., Spiegl and Langematz (2020)).

758   Also, please keep in mind the strong variability of the main pressure systems in the North Atlantic, which might wipe

759   out potential surface solar signals within a couple of months. Furthermore, and in our opinion, a physically sound

760   explanation for the alleged NAO-solar cycle phase coupling is missing so far. Thus, the claim that an inclusion of the

761   11-year solar cycle would lead to a better understanding of the decadal oscillations in the NH troposphere during

762   winter, is not supported by our analyses of the MiKlip historical ensemble simulations. We would finally like to note

763   that the detection of a significant decadal solar impact on the NAO in winter in the MPI-ESM-HR climate model, as

764   in other climate models, might to some degree suffer from the 'signal-to-noise paradox', i.e., a low strength of

765   predictable signals vs. a relatively high level of agreement between modelled and observed variability of the

hat gelöscht:

hat gelöscht: I

768 atmospheric circulation, which is particularly evident in the climate variability of the Atlantic sector (Scaife and Smith,

769 2018). Future studies with a distinct focus on the decadal prediction skill might help to confirm our results.

770

771 **Data availability**

772 The main numerical results will be made available upon request by the authors.

773 **Author contributions**

774 TS was in charge in conducting the analysis and writing the manuscript. UL initiated the study and contributed to

775 writing the manuscript. HP and JK were involved in conducting the MiKlip historical simulations and writing the

776 manuscript

777 **Competing interests**

778 The authors do not declare any competing interests.

779 **Acknowledgements**

780 We like to thank the DKRZ for granting the computational resources during MiKlip.

781 **Financial support**

782 BMBF funded projects MiKlip-2 (Förderkennzeichen 01LP1517A and 01LP1519A) and SOLCHECK

783 (Förderkennzeichen 01LG1906C)

784 **Review statement**

785 We would like to thank Wenjuan Huo and the anonymous reviewer for taking the time to carefully review our

786 manuscript.

787

788   **References**

789   Allan, R., and Ansell, T.: A new globally complete monthly historical gridded mean sea level pressure dataset

790   (HadSLP2): 1850–2004. J. Climate, 19(22), 5816-5842, doi.org/10.1175/JCLI3937.1, 2006.

791   Andrews, D. G.: Wave–mean-flow interaction in the middle atmosphere. In Adv. Geophys. (Vol. 28, pp. 249-275).

792   Elsevier, doi.org/10.1016/S0065-2687(08)60226-5, 1985.

793   Andrews, M. B., Knight, J. R., and Gray, L. J.: A simulated lagged response of the North Atlantic Oscillation to the

794   solar cycle over the period 1960–2009. Environ. Res. Lett., 10(5), 054022, doi10.1088/1748-9326/10/5/054022,

795   2015.

796   Arsenovic, P., Rozanov, E., Stenke, A., Funke, B., Wissing, J. M., Mursula, K., ... and Peter, T.: The influence of

797   Middle Range Energy electrons on atmospheric chemistry and regional climate. J Atmos Sol Terr Phys., 149,

798   180-190, doi.org/10.1016/j.jastp.2016.04.008, 2016.

799   Baldwin, M. P., and Dunkerton, T. J.: Stratospheric harbingers of anomalous weather regimes. Science, 294(5542),

800   581-584. doi:10.1126/science.1063315, 2001.

801   Baumgaertner, A. J., Jöckel, P., Riede, H., Stiller, G., and Funke, B.: Energetic particle precipitation in

802   ECHAM5/MESSy–Part 2: Solar proton events. Atmos. Chem. Phys., 10(15), 7285-7302, doi.org/10.5194/acp-

803   10-7285-2010, 2010.

804   Bodeker, G. E., Boyd, I. S., and Matthews, W. A.: Trends and variability in vertical ozone and temperature profiles

805   measured by ozonesondes at Lauder, New Zealand: 1986–1996. J. Geophys. Res., 103(D22), 28661-28681,

806   doi.org/10.1029/98JD02581, 1998.

807   Butchart, N.: The Brewer-Dobson circulation. Rev. Geophys., 52(2), 157-184,

808   https://doi.org/10.1002/2013RG000448, 2014.

809   Cagnazzo, C., Manzini, E., Giorgetta, M. A., Forster, P. M. D. F., and Morcrette, J. J.: Impact of an improved

810   shortwave radiation scheme in the MAECHAM5 General Circulation Model, Atmos. Chem. Phys., 7, 2503–

811   2515, https://doi.org/10.5194/acp-7-2503-2007, 2007.

Cionni, I., Eyring, V., Lamarque, J. F., Randel, W. J., Stevenson, D. S., Wu, F., ... and Waugh, D. W.: Ozone database in support of CMIP5 simulations: results and corresponding radiative forcing. Atmos. Chem. Phys., 11(21), 11267-11292, doi.org/10.5194/acp-11-11267-2011, 2011.

Chiodo, G., Calvo, N., Marsh, D. R., and Garcia-Herrera, R.: The 11year solar cycle signal in transient simulations from the Whole Atmosphere Community Climate Model. J. Geophys. Res., 117(D6), doi.org/10.1029/2011JD016393, 2012.

Chiodo, G., Oehrlein, J., Polvani, L. M., Fyfe, J. C., and Smith, A. K.: Insignificant influence of the 11-year solar cycle on the North Atlantic Oscillation. Nat. Geosci., 12(2), 94-99, doi.org/10.1038/s41561-018-0293-3, 2019.

Dhomse, S. S., Chipperfield, M. P., Feng, W., Hossaini, R., Mann, G. W., Santee, M. L. and Weber, M.: A single-peak-structured solar cycle signal in stratospheric ozone based on Microwave Limb Sounder observations and model simulations. Atmospheric Chemistry and Physics, 22(2), 903-916, doi.org/10.5194/acp-22-903-2022, 2022.

Drews, A., Huo, W., Matthes, K., Kodera, K., and Kruschke, T.: The Sun's role in decadal climate predictability in the North Atlantic. Atmos. Chem. Phys., 22(12), 7893-7904, doi.org/10.5194/acp-22-7893-2022, 2022.

Eyring, V., Lamarque, J. F., Hess, P., Arfeuille, F., Bowman, K., Chipperfiel, M. P., ... and Young, P. Y.: Overview of IGAC/SPARC Chemistry-Climate Model Initiative (CCMI) community simulations in support of upcoming ozone and climate assessments. SPARC newsletter, 40 (Januar), 48-66, 2013.

Forster, P. M., et al.: Evaluation of radiation scheme performance within chemistry climate models, J. Geophys. Res., 116, D10302, doi:10.1029/2010JD015361, 2011.

Fouquart, Y., and Bonnel, B.: Computations of solar heating of the earth's atmosphere—A new parameterization, Beitr. Phy. Atmos., 53, 35–62, 1980.

Gray, L. J., et al.: Solar influences on climate, Rev. Geophys., 48, RG4001, doi:10.1029/2009RG000282, 2010.

Gray, L. J., Scaife, A. A., Mitchell, D. M., Osprey, S., Ineson, S., Hardiman, S., ... and Kodera, K.: A lagged response to the 11 year solar cycle in observed winter Atlantic/European weather patterns. J. Geophys. Res., 118(24), 13-405, doi.org/10.1002/2013JD020062, 2013.

Gray, L. J., Woollings, T. J., Andrews, M. and Knight, J.: Eleven-year solar cycle signal in the NAO and Atlantic/European blocking. Q.J.R. Meteorol. Soc., 142: 1890-1903, https://doi.org/10.1002/qj.2782, 2016.

Huang, J., Hitchcock, P., Maycock, A. C., McKenna, C. M., and Tian, W.: Northern hemisphere cold air outbreaks are more likely to be severe during weak polar vortex conditions. Communications Earth and Environment, 2(1), 147. doi.org/10.1038/s43247-021-00215-6, 2021.

Iacono, M. J., Delamere, J.S., Mlawer, E.J., Shephard, M. W., Clough, S. A., and Collins, W. D.: Radiative forcing by long-lived greenhouse gases: Calculations with the AER radiative transfer models, J. Geophys. Res., 113, D13103, doi:10.1029/2008JD009944, 2008.

Ilyina, T., Six, K. D., Segschneider, J., Maier-Reimer, E., Li, H., and Núñez-Riboni, I.: Global ocean biogeochemistry model HAMOCC: Model architecture and performance as component of the MPI-Earth system model in different CMIP5 experimental realizations. J. Adv. Model. Earth Syst., 5(2), 287-315, doi.org/10.1029/2012MS000178, 2013.

Ineson, S., Scaife, A. A., Knight, J. R., Manners, J. C., Dunstone, N. J., Gray, L. J., and Haigh, J. D.: Solar forcing of winter climate variability in the Northern Hemisphere. Nat. Geosci., 4(11), 753-757, doi.org/10.1038/ngeo1282, 2011.

Jackman, C. H., Marsh, D. R., Vitt, F. M., Garcia, R. R., Randall, C. E., Fleming, E. L. and Frith, S. M.: Long-term middle atmospheric influence of very large solar proton events. J. Geophys. Res, 114(D11), doi.org/10.1029/2008JD011415, 2009.

Jungclaus, J. H., Fischer, N., Haak, H., Lohmann, K., Marotzke, J., Matei, D., ... and Von Storch, J. S.: Characteristics of the ocean simulations in the Max Planck Institute Ocean Model (MPIOM) the ocean component of the MPI-Earth system model. J. Adv. Model. Earth Syst., 5(2), 422-446, doi.org/10.1002/jame.20023, 2013.

Kodera, K.: Solar cycle modulation of the North Atlantic Oscillation: Implication in the spatial structure of the NAO. Geophys. Res. Lett, 29(8), 59-1, doi.org/10.1029/2001GL014557, 2002.

Kodera, K., and Kuroda, Y.: Dynamical response to the solar cycle. J. Geophys. Res., 107(D24), doi.org/10.1029/2002JD002224, ACL-5. 2002.

863 Kuroda, Y., Kodera, K., Yoshida, K., Yukimoto, S., & Gray, L.: Influence of the solar cycle on the North Atlantic

864 Oscillation. J. Geophys. Res., 127(1), e2021JD035519, doi.org/10.1029/2021JD035519, 2022.

865 Langematz, U., Kubin A., Brühl, C., Baumgaertner, A.J.G., Cubasch, U., and Spangehl, T.: Solar effects on

866 chemistry and climate including ocean interactions, in Climate And Weather of the Sun-Earth System

867 (CAWSES): Highlights from a Priority Program, F.-J. Lübken, ed., Springer, Dordrecht, The Netherlands, 2013.

868 Lean, J.: Evolution of the Sun's spectral irradiance since the Maunder Minimum. Geophys. Res. Lett., 27(16), 2425-

869 2428, doi.org/10.1029/2000GL000043, 2000.

870 Ma, H., Chen, H., Gray, L., Zhou, L., Li, X., Wang, R. and Zhu, S.: Changing response of the North

871 Atlantic/European winter climate to the 11-year solar cycle. Environ. Res. Lett., 13(3), 034007,

872 doi10.1088/1748-9326/aa9e94, 2018.

873 Marotzke, J., Müller, W. A., Vamborg, F. S., Becker, P., Cubasch, U., Feldmann, H., ... and Ziese, M.: MiKlip: a

874 national research project on decadal climate prediction. Bull. Am. Meteorol. Soc., 97(12), 2379-2394,

875 https://doi.org/10.1175/BAMS-D-15-00184.1, 2016.

876 Matthes, K., Langematz, U., Gray, L. L., Kodera, K., and Labitzke, K.: Improved 11-year solar signal in the Freie

877 Universität Berlin climate middle atmosphere model (FUB-CMAM). J. Geophys. Res., 109(D6),

878 doi.org/10.1029/2003JD004012, 2004.

879 Matthes, K., Kuroda, Y., Kodera, K., and Langematz, U.: Transfer of the solar signal from the stratosphere to the

880 troposphere: Northern winter. J. Geophys. Res., 111(D6), doi.org/10.1029/2005JD006283, 2006.

881 Matthes, K., Funke, B., Andersson, M. E., Barnard, L., Beer, J., Charbonneau, P., Clilverd, M. A., Dudok de Wit, T.,

882 Haberreiter, M., Hendry, A., Jackman, C. H., Kretzschmar, M., Kruschke, T., Kunze, M., Langematz, U.,

883 Marsh, D. R., Maycock, A. C., Misios, S., Rodger, C. J., Scaife, A. A., Seppälä, A., Shangguan, M., Sinnhuber,

884 M., Tourpali, K., Usoskin, I., van de Kamp, M., Verronen, P. T., and Versick, S.: Solar forcing for CMIP6

885 (v3.2), Geosci. Model Dev., 10, 2247–2302, doi.org/10.5194/gmd-10-2247-2017, 2017.

886 Meehl, G. A., J. M. Arblaster, G. Branstator, and H. van Loon: A Coupled Air–Sea Response Mechanism to Solar

887 Forcing in the Pacific Region. J. Climate, 21, 2883–2897, https://doi.org/10.1175/2007JCLI1776.1, 2008.

hat gelöscht: Marsh, D. R., Garcia, R. R., Kinnison, D. E., Boville, B. A., Sassi, F., Solomon, S. C., and Matthes, K.: Modeling the whole atmosphere response to solar cycle changes in radiative and geomagnetic forcing. J. Geophys. Res., 112(D23), doi.org/10.1029/2006JD008306, 2007.¶

893   Meehl, G. A., Goddard, L., Boer, G., Burgman, R., Branstator, G., Cassou, C., ... and Yeager, S.; Decadal climate

894   prediction: an update from the trenches. Bull. Am. Meteorol. Soc., 95(2), 243-267, doi.org/10.1175/BAMS-D-

895   12-00241.1, 2014.

896   Mehta, V., Meehl, G., Goddard, L., Knight, J., Kumar, A., Latif, M., ... and Stammer, D.: Decadal climate

897   predictability and prediction: where are we?. Bull. Am. Meteorol. Soc., 92(5), 637-640,

898   doi.org/10.1175/2010BAMS3025.1, 2011.

899   Misios, S. and Schmidt, H.: Mechanisms Involved in the Amplification of the 11-yr solar cycle signal in the tropical

900   Pacific Ocean, J. Climate, 25, 5102–5118, doi.org/10.1175/JCLID-11-00261.1, 2012.

901   Müller, W. A., Jungclaus, J. H., Mauritsen, T., Baehr, J., Bittner, M., Budich, R., ... and Marotzke, J: A higher-

902   resolution version of the max planck institute earth system model (MPI-ESM1. 2-HR). J. Adv. Model. Earth

903   Syst., 10(7), 1383-1413, doi.org/10.1029/2017MS001217, 2018.

904   Paulsen, H., Ilyina, T., Six, K. D., and Stemmler, I.: Incorporating a prognostic representation of marine nitrogen

905   fixers into the global ocean biogeochemical model HAMOCC. J. Adv. Model. Earth Syst., 9(1), 438-464,

906   doi.org/10.1002/2016MS000737, 2017.

907   Pohlmann, H., Müller, W. A., Kulkarni, K., Kameswarrao, M., Matei, D., Vamborg, F. S. E., Kadow, C., Illing, S.,

908   and Marotzke, J.: Improved forecast skill in the tropics in the new MiKlip decadal climate predictions, Geophys.

909   Res. Lett., 40, 5798– 5802, doi.10.1002/2013GL058051, 2013.

910   Pohlmann, H., Müller, W. A., Bittner, M., Hettrich, S., Modali, K., Pankatz, K., and Marotzke, J.: Realistic quasi-

911   biennial oscillation variability in historical and decadal hindcast simulations using CMIP6 forcing. Geophys.

912   Res. Lett., 46(23), 14118-14125, doi.org/10.1029/2019GL084878, 2019.

913   Randel, W. J., Smith, A. K., Wu, F., Zou, C., and Qian, H.: Stratospheric Temperature Trends over 1979–2015

914   Derived from Combined SSU, MLS, and SABER Satellite Observations, J. Climate, 29(13), 4843-4859,

915   doi.org/10.1175/JCLI-D-15-0629.1, 2016.

916   Reick, C. H., Raddatz, T., Brovkin, V., and Gayler, V.: Representation of natural and anthropogenic land cover

917   change in MPI-ESM. J. Adv. Model. Earth Syst., 5(3), 459-482, doi.org/10.1002/jame.20022, 2013.

Scaife, A. A., Ineson, S., Knight, J. R., Gray, L., Kodera, K., and Smith, D. M.: A mechanism for lagged North Atlantic climate response to solar variability. Geophys. Res. Lett., 40(2), 434-439, doi.org/10.1002/grl.50099, 2013.

Scaife, A. A. and Smith, D.: A signal-to-noise paradox in climate science. NPJ Climate and Atmospheric Science, 1(1), 28, doi:10.1038/s41612-018-0038-4, 2018.

Seppälä, A., Randall, C. E., Clilverd, M. A., Rozanov, E., & Rodger, C. J.: Geomagnetic activity and polar surface air temperature variability. J. Geophys. Res, 114(A10), doi.org/10.1029/2008JA014029, 2009.

Seppälä, A., Matthes, K., Randall, C. E. and Mironova, I. A.: What is the solar influence on climate? Overview of activities during CAWSES-II. Progress in Earth and Planetary Science, 1(1), 1-12, doi.org/10.1186/s40645-014-0024-3, 2014.

Schmidt, H., Brasseur, G. P., and Giorgetta, M. A.: Solar cycle signal in a general circulation and chemistry model with internally generated quasi-biennial oscillation. J. Geophys. Res.,115(D1), doi.org/10.1029/2009JD012542, 2010.

Spiegl, T. and Langematz, U.: Twenty-First-Century Climate Change Hot Spots in the Light of a Weakening Sun. Journal of Climate, 33(9), 3431-3447, doi.org/10.1175/JCLI-D-19-0059.1, 2020.

Stevens, B., et al.: Atmospheric component of the MPI-M Earth System Model: ECHAM6, J. Adv. Model. Earth Syst., 5, 146–172, doi:10.1002/jame.20015, 2013.

Taylor, K. E., Stouffer, R. J., and Meehl, G. A.: An overview of CMIP5 and the experiment design. Bull. Am. Meteorol. Soc., 93(4), 485-498. doi.org/10.1175/BAMS-D-11-00094.1, 2012.

Thiéblemont, R., Matthes, K., Omrani, N. E., Kodera, K., and Hansen, F.: Solar forcing synchronizes decadal North Atlantic climate variability. Nat. Commun., 6(1), 8268, doi:10.1038/ncomms9268, 2015.